Supporting Information

In situ Fabrication and Reactivation of Highly Selective and Stable Ag Catalysts for Electrochemical CO_2 Conversion

Ming Ma,[1]* Kai Liu,[1] Jie Shen,[2] Recep Kas[1] and Wilson A. Smith[1]*

[1]Materials for Energy Conversion and Storage (MECS), Department of Chemical Engineering, Delft University of Technology, Van der Maasweg 9, 2629 HZ, Delft, The Netherlands

[2]QuTech and Kavli Institute of Nanoscience, Delft University of Technology, Delft 2600 GA, The Netherlands

Corresponding authors

*E-mail: m.ma.cn@outlook.com (M.M.).

*E-mail: W.Smith@tudelft.nl (W.A.S.).

Chemicals: All chemicals were used as received: Silver foil (99.998%, 0.25 mm thick, hard) was purchased from Alfa Aesar. Silver foils were ultrasonically cleaned in acetone and ethanol, and then were dried with nitrogen gas. K_2CO_3 (99.99%), KOH (99.99%), K_2HPO_4 and KCl (≥99%) were purchased from Sigma Aldrich. All chemicals were used without any purification. Before electrolysis, CO_2-saturated $KHCO_3$ solutions were prepared by bubbling CO_2 gas through K_2CO_3 solutions. Water with resistivity of 18.2 MΩ cm from Milli-Q® integral ultrapure water (Merck Millipore) was used in this work.

Fabrication of Ag_2CO_3 on Ag foil: A piece of Ag foil was immersed in CO_2-saturated $KHCO_3$ solutions in a two-compartment cell (the two-compartment cell was separated by a Nafion-115 proton exchange membrane) with a Pt counter electrode and an Ag/AgCl reference electrode (XR300, saturated KCl + AgCl solution (KS120), Radiometer Analytical). Ag foil electrodes was anodic-etched at a potential of 2.6 V vs. RHE for 3 min in CO_2-saturated 0.1 M $KHCO_3$ electrolytes to form Ag_2CO_3 layers. The possible reaction for Ag_2CO_3 formation by anodic-etching of Ag foil in $KHCO_3$ as below

$$2Ag + 2H_2O + HCO_3^- \rightarrow Ag_2CO_3 + 6e^- + O_2\uparrow + 5H^+ \quad (1)$$

Electrocatalytic CO_2 reduction measurement

The electrochemical reduction of CO_2 on AE-Ag and untreated polycrystalline Ag was performed in CO_2-saturated 0.1 M $KHCO_3$ (pH 6.83) at ambient temperature and pressure in an electrochemical cell. The cell consists of working and counter electrode compartments, separated by a Nafion-115 proton exchange membrane to avoid the oxidation of the products of CO_2 reduction. The working compartment was continuously purged with CO_2, directly venting into the gas-sampling loop of a gas chromatograph (GC) for periodic quantification of the gas-phase products.

Physical Characterization: Scanning electron microscope (SEM Hitachi S4800) and transmission electron microscopy (JEOL JEM3200-FSC TEM) were used to characterize the morphology and nanostructure of the samples. The X-ray diffraction (XRD) patterns of the samples were performed by using a diffractometer (Bruker AXS GmbH-D8 Discover) with Co-Kα radiation (λ = 1.78886 Å). The surface composition of the samples were detected by X-ray photoelectron spectroscopy (XPS, Thermo Scientific™ K-Alpha™). Surface valence band XPS measurements were also performed with a Thermo Scientific K-alpha apparatus

using an Al K-ray source and a flood Gun. 50 scans in the valence band binding energy range (0-30 eV) were performed with a spot size of 400 μm, pass energy of 50 eV, dwell time of 50 ms and a step size of 0.1 eV.

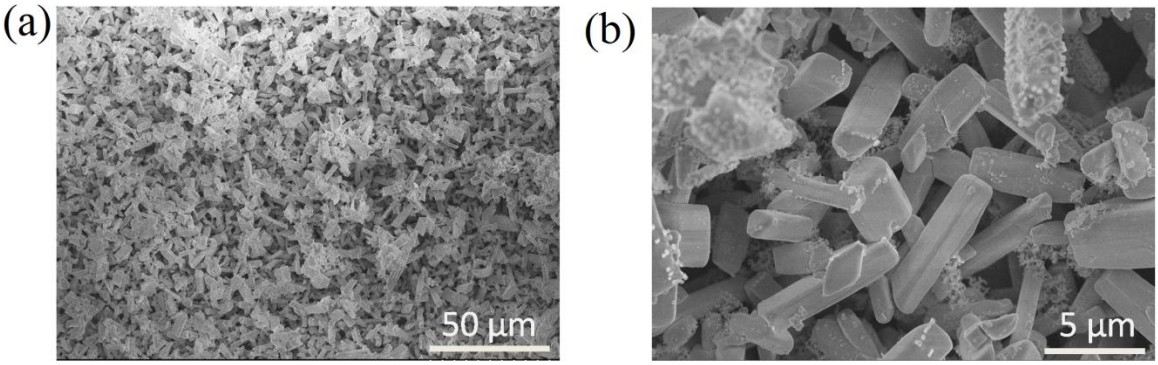

Figure S1. SEM image of anodic-etched Ag before CO_2 reduction electrolysis (a) and related magnified image (b) .

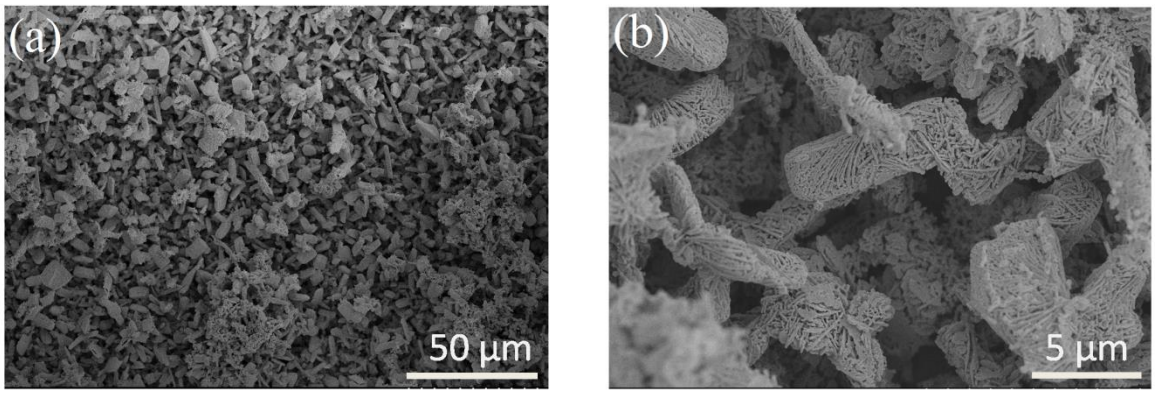

Figure S2. SEM images of anodic-etched Ag after CO_2 reduction electrolysis (a) and related magnified image (b) .

.

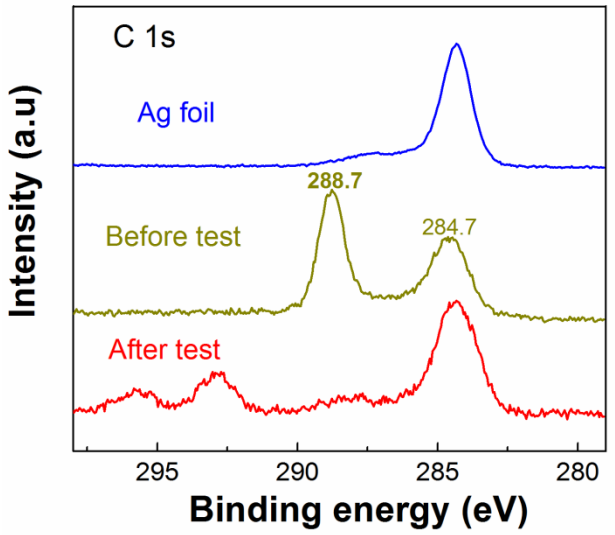

Figure S3. XPS spectra of C1s of the polycrystalline Ag electrode (blue line) and anodic-etched Ag electrode before (dark yellow line) and after (red line) CO_2 reduction electrolysis, respectively (After electrolysis, the binding energy of 293 eV and 295.5 eV represents the peak of K $2p_{3/2}$ and K $2p_{1/2}$, respectively,[1] and potassium element was derived from $KHCO_3$ electrolytes).

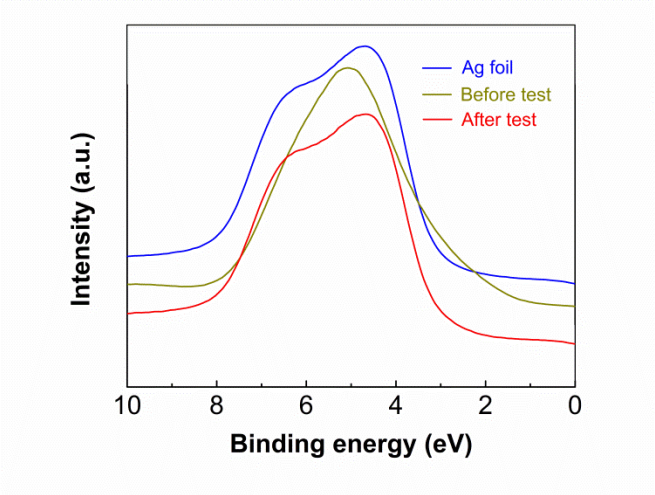

Figure S4. Comparison of surface valence band XPS spectra of Ag foil (blue line) and anodic-etched Ag before (dark yellow line) and after (red line) CO_2 electrolysis. (valence band XPS spectrum of anodic etched Ag after electrolysis is consistent with that of metallic Ag foil).

Calculation of the thickness of anodic-etched Ag

The total number (mole) of Ag_2CO_3 molecule formed on Ag foil could be estimated by the following equation:

$$N = \frac{Q}{nF} \quad (2)$$

where, Q is the total charge (4.14 C for 3 min anodic-etching) used for the electroreduction of Ag_2CO_3 at the initial stage of electrolysis (Figure S5d), and n is the number of electron required for the electroreduction of one Ag_2CO_3 molecule (here, n is 2). F is Faraday constant (96485 C/mol). Thus, the total number of carbon atom from Ag_2CO_3 is 2.15×10^{-5} mol, which is even much lower than CO (3.36×10^{-5} mol) produced in CO_2 reduction for 1 h at -0.55 V vs. RHE. Therefore, the carbon source for CO_2 reduction is not from Ag_2CO_3 in this work.

The thickness (d) of the Ag_2CO_3 layer formed on Ag foil can be estimated by the following equation:

$$d = \frac{NM}{\rho A} \quad (3)$$

where, M and ρ are molar mass (275.75 g/mol) and the mass density (ρ = 6.077 g/cm^3) of Ag_2CO_3, respectively. The N is the total number of Ag_2CO_3 molecule (equation (2), and A is the electrode size used for electrolysis (~2 cm^2). Thus, the equation (3) can be rewritten as:

$$d = \frac{QM}{nF\rho A} \quad (4)$$

We can get the total charge used for the electroreduction of Ag_2CO_3 according to the initial high current in Figure S5. $Q_{0.5\ min}$, $Q_{1\ min}$, $Q_{2\ min}$ and $Q_{3\ min}$ are 0.49 C, 1.41 C, 3.01 C and 4.14 C, respectively. Thus, the thickness of anodic-etched Ag was estimated in Table S1. Here, the thickness of nanoporous Ag is identical to the corresponding Ag_2CO_3 film thickness.

Table S1. The average thickness of nanoporous Ag under different fabrication time.

Anodic-etching time (min)	Q (C)	Thickness of nanoporous Ag (μm)
0.5	0.49	0.6
1	1.41	1.7
2	3.01	3.5
3	4.14	4.9

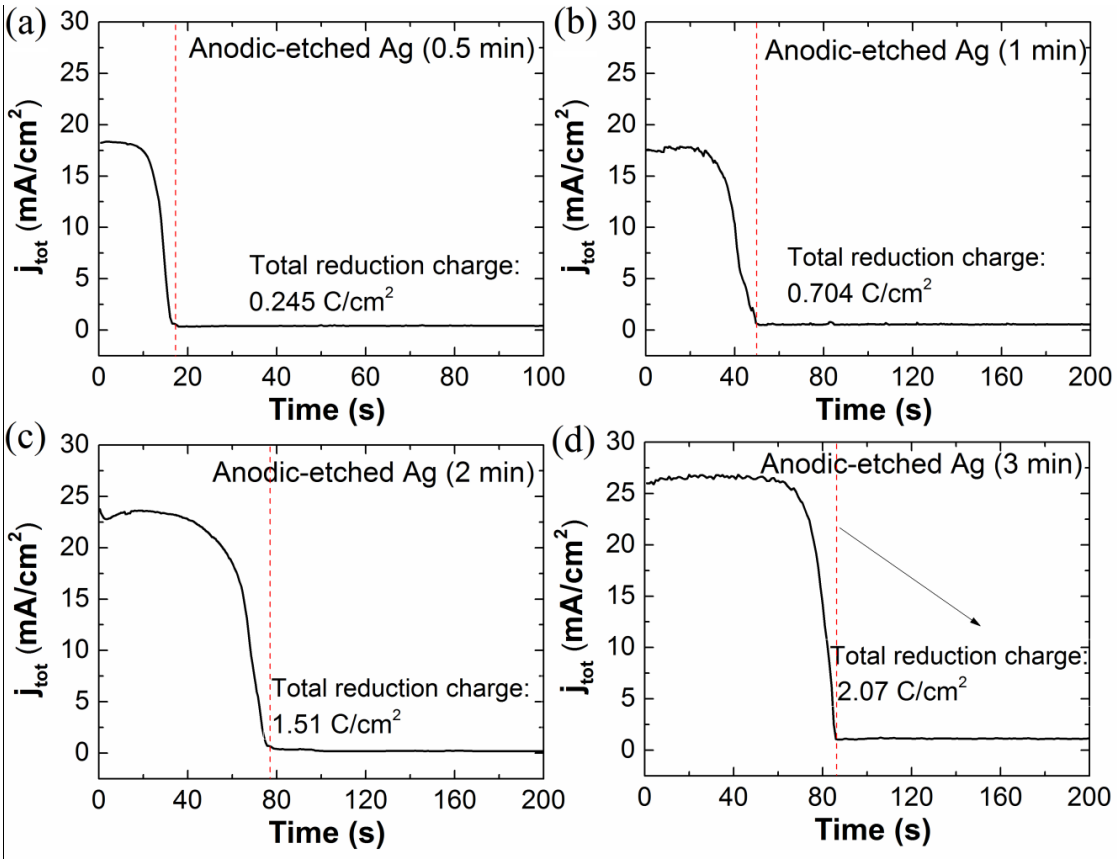

Figure S5. Current densities as a function of time for anodic-etched Ag with different fabriation time of (a) 0.5 min, (b) 1 min, (c) 2 min and (d) 3 min for CO_2 electroreduction at -0.55 V vs. RHE in CO_2-saturated 0.1 M $KHCO_3$ electrolytes.

Faradaic efficiency for H_2

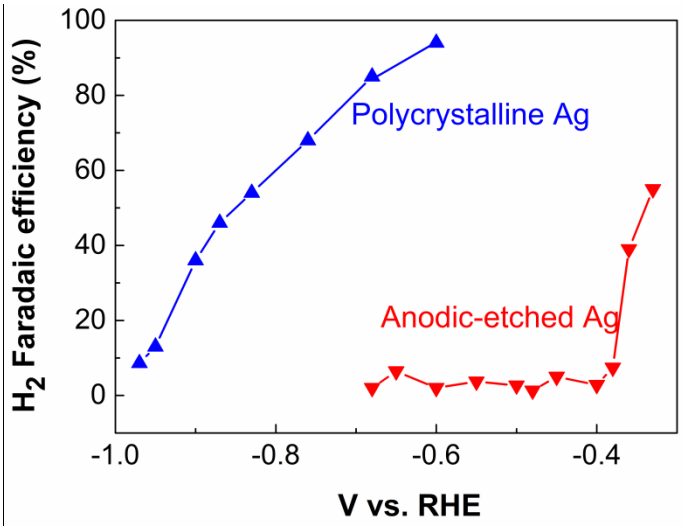

Figure S6. Comparison of Faradaic efficiency for H_2 of untreated polycrystalline Ag and anodic-etched Ag at various potentials in CO_2-saturated 0.1 M $KHCO_3$ (pH 6.8).

Summary of high selective and stable electrocatalysts

Table S2. Summary of CO_2 reduction performances on Ag catalysts at a potential of -0.4 V vs. RHE in CO_2-saturated bicarbonate electrolyte.

Sample	V vs. RHE	CO FE (%)	J_{tot} (mA/cm^2)	Electrolyte
an-Ag[2]	-0.4	~30%	Not reported	
mesostructured Ag[3]	-0.4	Not reported	Not reported	
nanostructured Ag[4]	-0.4	Not reported	Not reported	
air-annealed Ag[5]	-0.4	~10%	Not reported	
OD-Ag[6]	-0.4	12%	~0.034	0.1 M $KHCO_3$
Ag nanocoral [7]	-0.4	~75%	<1	0.1 M $KHCO_3$
Nanoporous Ag[8]	-0.4	79%	3.3	0.5 M $KHCO_3$
Ag nanoparticles[9]	-0.4	50%	Not reported	0.5 M $KHCO_3$
AE-Ag (this work)	**-0.4**	**>92%**	**~0.23**	0.1 M $KHCO_3$

(The superscripted numbers are the citations.**)**

Table S3. Summary of CO_2 reduction performances on highly selective and stable electrocatalysts in CO_2-saturated bicarbonate electrolyte.

Sample	V vs. RHE	CO FE (%)	J_{tot} (mA/cm^2)	Stability (hours)
OD-Cu[10]	-0.5	40%	2.7	7 h
OD-Au[11]	-0.4	98%	~10	8 h
OD-Au[12]	-0.4	90%	>1	18 h
OD-Ag[6]	-0.6	80%	>0.3	2 h
Reduced SnO_2 Porous Nanowires[13]	-0.8	< 20 %	<6	15 h
Au Nanowires[14]	-0.4	95%	>4	6 h
Au needles[15]	−0.35	95%	~15	8 h
N-doped CNT[16]	-0.8	80%	<1	10 h
Nanoporous Ag[8]	-0.4	79%	3.3	2 h
Ag nanoparticles[9]	-0.75	84.4%	~4	
AE-Ag (this work)	**-0.55**	**>90%**	**~1**	**>100 h (with 3 min in-situ reactivation)**

Table S4. Summary of CO_2 reduction performances on bimetallic electrocatalysts in CO_2-saturated bicarbonate electrolyte.

Sample	V vs. RHE	CO FE (%)	J_{tot} (mA/cm^2)	Stability (hours)
OD Cu-In[17]	-0.6	85	~0.5	7 h
OD Cu-Sn[18]	-0.6	90	1	14 h
Cu NW-Sn[19]	-0.7	82	3	6 h
Porous Cu_3-Pd_7[20]	-0.8	>80	<1	
Cu_{15}-Pd_{85} NPs[21]	-0.6	>60	~1.5	
CoPc/CNT hybrid[22]	-0.63	>90%	10	10 h
Ag-In[23]	-0.6	< 45%	<0.5	4 h

Electrochemical active surface area

The electrochemical active surface areas of Ag electrodes were determined by using a monolayer oxidation method in a three-electrode electrochemical cell with a platinum counter electrode and Ag/AgCl reference electrode.[24] As shown in Figure S7a, a current density peak was observed at about 1.15 V vs RHE, which corresponds to a monolayer of silver oxide or AgOH formation.[24] The measurement was performed in 0.1 M KOH electrolytes with bubbling N_2. Firstly, the Ag electrodes were reduced at −0.4 V vs RHE for 10 min in order to reduce any existing oxide layer on Ag electrodes, and then immediately oxidized by a constant potential of 1.15 V vs RHE to form only a monolayer of oxide on the Ag surface (Figure S7a). By measuring the charge used during the oxidation process, relative active surface area could be calculated for the Ag catalysts.[24]

The EASA can be obtained by normalizing the charge value to that of polycrystalline Ag foil (the EASA of polycrystalline Ag is used as the standard reference), thus Ag catalysts resulting from Anodic-etched Ag with 0.5 min, 1 min, 2 min and 3min correspond to the EASA of 2.6, 5, 9.45 and 11.6.

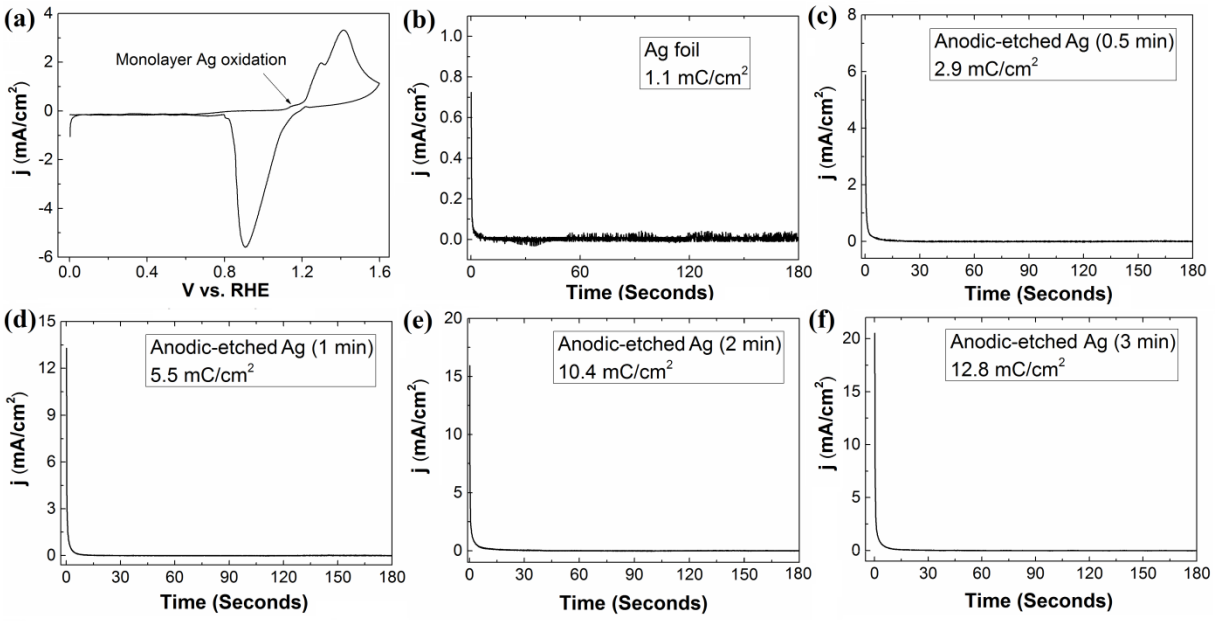

Figure S7. (a) A cyclic voltammetry of polycrystalline Ag foils in 0.1 M KOH electrolytes at ambient temperature and pressure (scan rate is 0.02 V/s). Current density as a function of time at constant potential of 1.15 V vs. RHE 0.1 M KOH electrolytes for Ag foil (b) and Ag with anodic-etch of (c) 0.5 min, (d) 1 min, (e) 2 min and (f) 3 min, respectively.

Partial current density and the normalized CO partial current density by EASA

The partial current density for CO is calculated by a potential as below:

$$j_{CO} = f \times j_{tot} \quad (5)$$

where j_{CO}, f and j_{tot} are the partial current density, Faradaic efficiency for CO production and the total current density, respectively.

Thus, at -0.55 V vs. RHE, the normalized j_{co} by EASA for anodic-etched Ag is ~ 0.08 mA/cm^2, which is ~ 40 fold bigger than that (~ 0.002 mA/cm^2) of untreated Ag (the EASA of polycrystalline Ag is used as standard reference).

Bicarbonate concentration effect

The electrocatalytic reduction of CO_2 were performed at a constant potential (-0.4 V vs. RHE) at $KHCO_3$ concentrations ranging from 0.5 to 0.1 M. KCl was added to the low $KHCO_3$ concentration solutions for getting a total concentration of 0.5 M, keeping ionic strength of electrolytes.

Current density and partial current density

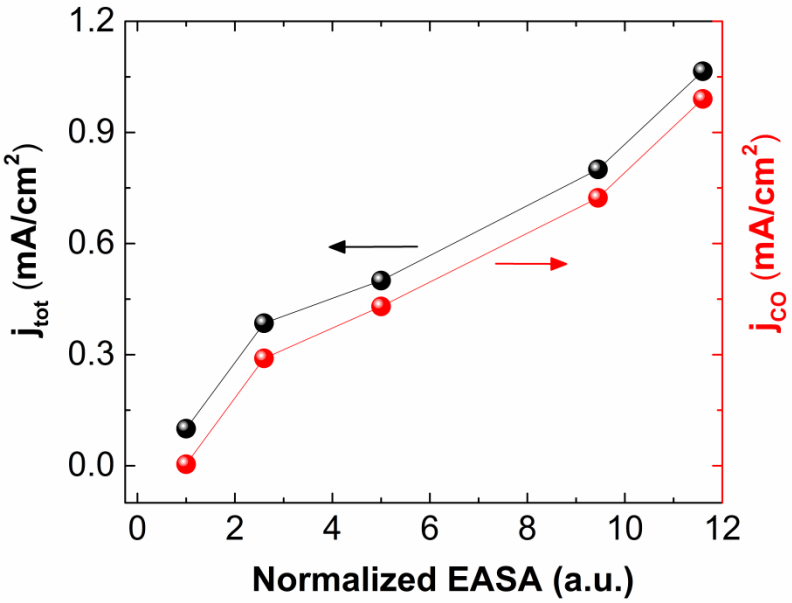

Figure S8. Geometric current density and partial current density for CO as a function of normalized EASA.

Electrochemical impedance spectroscopy measurement

Electrochemical impedance spectroscopy (EIS) measurements were performed in a three-electrode cell. The cell was filled with 0.1M $KHCO_3$ aqueous solution saturated with CO_2. During the experiments, the electrolyte was bubbled with CO_2 at the surface to avoid the escape of CO_2, dissolution of other gases and the disturbance caused by the bubbles. The impedance spectra were recorded using a potentiostat (Princeton, PARSTAT MC) in a frequency range from 100 KHz to 10 mHz at different potentials with an amplitude of 10 mV. Charge transfer resistance between untreated Ag and Ag_2CO_3-derived Ag as a function of overpotential was extracted from EIS based on the equivalent circuit using ZView software.

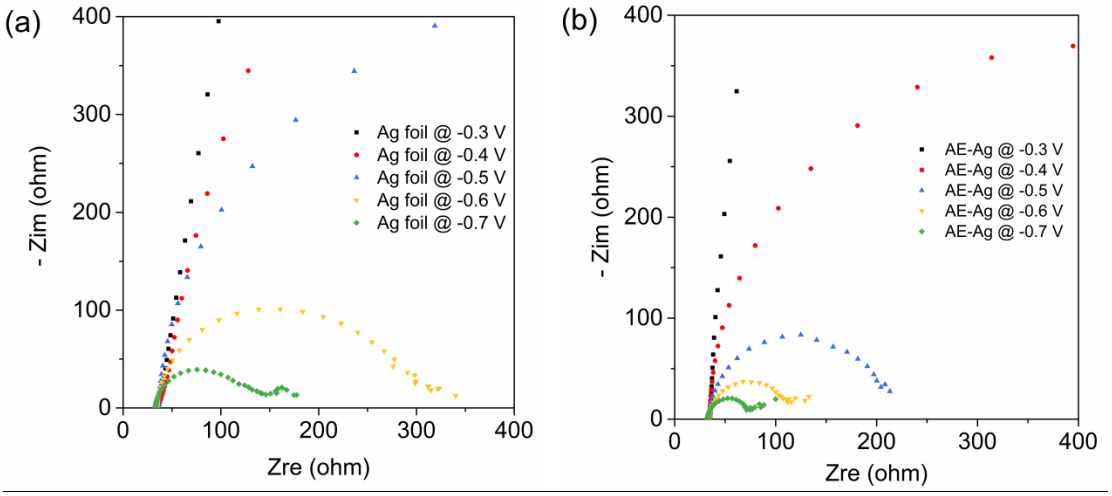

Figure S9. Nyquist plots of Ag foil (a) and anodic-etched Ag (b) at various potentials in 0.1M $KHCO_3$ aqueous solution saturated with CO_2.

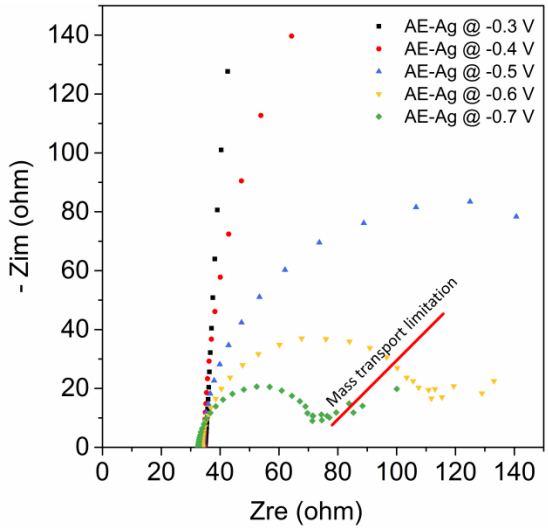

Figure S10. Magnified Nyquist plots of anodic-etched Ag in 0.1M $KHCO_3$ aqueous solution saturated with CO_2.

OH^- adsorption/desorption study:

Researchers have previously studied the adsorption and desorption of OH^- ions on single crystalline Ag (such as (111), (100) and (110)) by performing cyclic voltammetry curves in 0.1 M KOH or 0.1 M NaOH, showing the difference in recorded peak potentials with the distinct facets of Ag electrodes in the 'double layer' potential region, which indicates that crystal facets of Ag electrodes could significantly influence the OH^- adsorption/desorption process in the potential range from ~-0.3 V to ~1 V (double layer region) at room temperature.[25–27] In order to reveal the variation of Ag surface facets before and after anodic-treatment, the OH^- adsorption/desorption process has been performed in argon-purged 0.1 M KOH. Firstly, the Ag electrodes were reduced at −0.4 V vs RHE for 10 min for reducing any existing oxide layer on Ag electrodes, and then immediately performed cyclic voltammetry in argon-purged 0.1 M KOH (here, AE-Ag was reduced to metallic Ag in CO_2-saturated 0.1 M $KHCO_3$ before immersing in 0.1 M KOH).

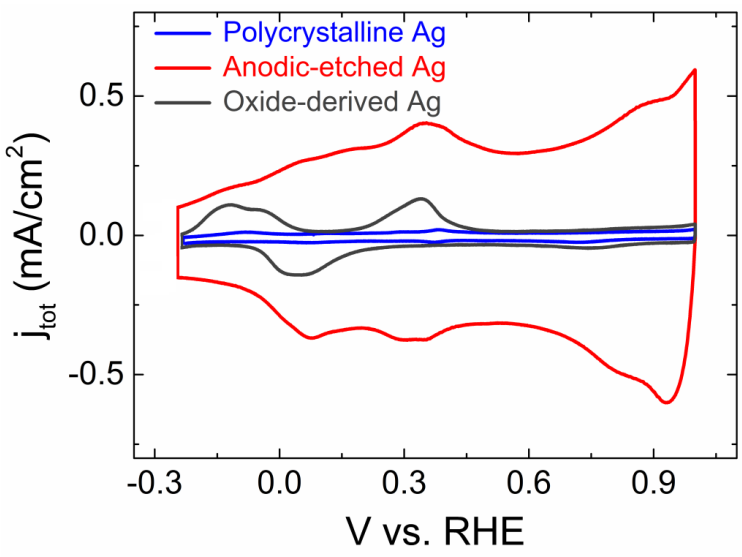

Figure S11. Cyclic voltammetry curves of the polycrystalline Ag electrode (blue line), anodic-etched Ag (red line) and oxide-derived Ag (dark gray line) in argon-purged 0.1 M KOH electrolyte. All cyclic voltammograms were performed at room temperature with a sweep rate of 50 mV/s.

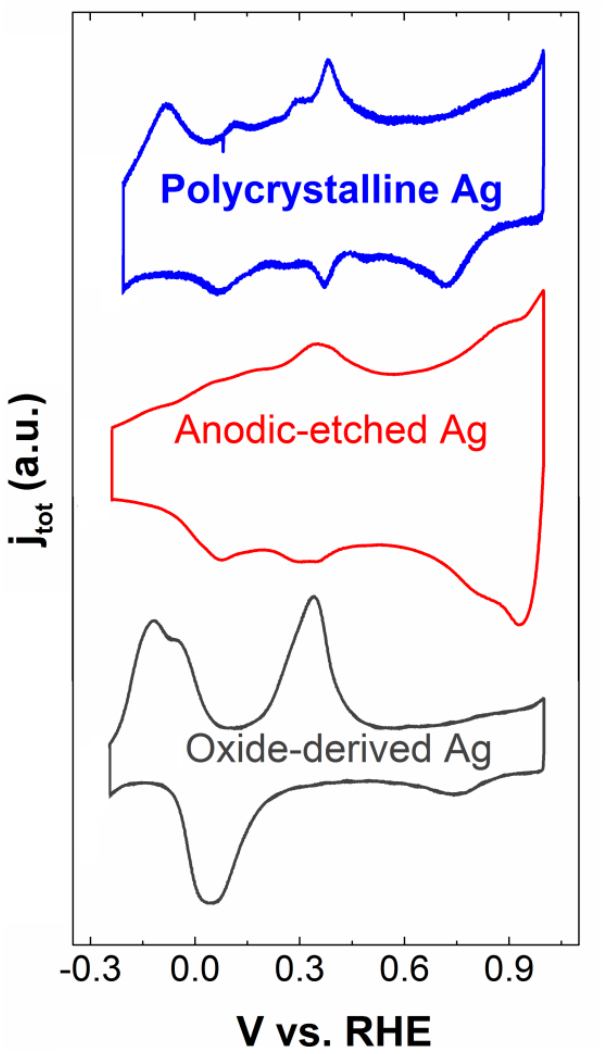

Figure S12. The cyclic voltammetry curves of the polycrystalline Ag electrode (blue line), anodic-etched Ag (red line) and oxide-derived Ag (dark gray line) with current density in arbitrary units (argon-purged 0.1 M KOH electrolyte).

IR correction of potentials

In this work, the potentiostatic electrochemical impedance spectroscopy (PEIS) was used to determine the solution resistance (Rs) as shown Figure S10 in the SI. The Rs has slightly changed from 35 Ω at -0.903 V vs. Ag/AgCl to 33 Ω at -1.315V vs. Ag/AgCl. In addition, the IR determination function of potentiostat (Princeton, VersaSTAT 3 Potentiostat Galvanostat) was used, revealing that the value of Rs was 33 Ω. Thus, the Rs of 33 Ω was applied for IR drop calculation.

After measuring the current at various potentials, the IR drop and corrected voltage can be calculated, as shown in the below table S5. At lese negative potentials than -1.065 vs. Ag/AgCl, the IR drop was negligible due to the very low current. The relatively higher current at more negative potentials was companied with significant IR drop, as shown in the below Table S5.

Table S5. IR drop and corrected voltage for anodic-etched Ag (4.9 μm).

V vs. Ag/AgCl	Current (mA)	IR drop (V)	Corrected V vs. RHE
-0.903	0.033	0.001	-0.300
-0.933	0.037	0.001	-0.330
-0.96	0.059	0.002	-0.356
-0.986	0.125	0.004	-0.380
-1.009	0.2165	0.007	-0.400
-1.065	0.401	0.0132	-0.450
-1.113	1.015	0.0345	-0.478
-1.163	1.47	0.05	-0.51
-1.219	2	0.06	-0.551
-1.265	2.9	0.095	-0.567
-1.315	3.2	0.106	-0.607

Error bars for CO Faradaic efficiency

The points of CO Faradaic efficiency were added with error bars which correspond to the standard deviation of repeated gas measurements.

Table S6. The average Faradaic efficiency of anodic-etched Ag (4.9 μm) at various potentials.

iR Corrected V vs. RHE	CO FE (%)	Standard Deviation (%)
-0.3	14.8	0.47
-0.33	45	1.96
-0.36	60.2	2.51
-0.38	84	4
-0.4	92.36	3.22
-0.45	93.7	3.33
-0.48	93.3	3.1
-0.5	94.2	3.62
-0.55	92.5	3.48
-0.57	92	3.07
-0.61	96.2	3.51

Table S7. The average Faradaic efficiency of Ag foil at various potentials.

iR Corrected V vs. RHE	CO FE (%)	Standard Deviation (%)
-0.97	86	1.1
-0.95	76	3.5
-0.9	60.8	2.58
-0.87	50	1.58
-0.83	37.6	2.8
-0.76	22.5	2.4
-0.68	12	1.22
-0.60	4.1	0.4
-0.55	3.4	0.4

REFERENCES

(1) Mikhlin, Y.; Karacharov, A.; Tomashevich, Y.; Shchukarev, A. *Vacuum* **2016**, *125*, 98–105.

(2) Zhou, L. Q.; Ling, C.; Jones, M.; Jia, H. *Chem. Commun.* **2015**, *51* (100), 17704–17707.

(3) Yoon, Y.; Hall, A. S.; Surendranath, Y. *Angew. Chemie - Int. Ed.* **2016**, *55* (49), 15282–15286.

(4) Jee, M. S.; Jeon, H. S.; Kim, C.; Lee, H.; Koh, J. H.; Cho, J.; Min, B. K.; Hwang, Y. J. *Appl. Catal. B Environ.* **2016**, *180*, 372–378.

(5) Jiang, K.; Kharel, P.; Peng, Y.; Gangishetty, M. K.; Lin, H.-Y. G.; Stavitski, E.; Attenkofer, K.; Wang, H. *ACS Sustain. Chem. Eng.* **2017**, *5* (10), 8529–8534.

(6) Ma, M.; Trześniewski, B. J.; Xie, J.; Smith, W. A. *Angew. Chemie Int. Ed.* **2016**, *55* (33), 9748–9752.

(7) Hsieh, Y.-C.; Senanayake, S. D.; Zhang, Y.; Xu, W.; Polyansky, D. E. *ACS Catal.* **2015**, *5* (9), 5349–5356.

(8) Lu, Q.; Rosen, J.; Zhou, Y.; Hutchings, G. S.; Kimmel, Y. C.; Chen, J. G.; Jiao, F. *Nat. Commun.* **2014**, *5*, 3242.

(9) Kim, C.; Jeon, H. S.; Eom, T.; Jee, M. S.; Kim, H.; Friend, C. M.; Min, B. K.; Hwang, Y. J. *J. Am. Chem. Soc.* **2015**, *137* (43), 13844–13850.

(10) Li, C. W.; Kanan, M. W. *J. Am. Chem. Soc.* **2012**, *134* (17), 7231–7234.

(11) Chen, Y.; Li, C. W.; Kanan, M. W. *J. Am. Chem. Soc.* **2012**, *134* (49), 19969–19972.

(12) Schreier, M.; Curvat, L.; Giordano, F.; Steier, L.; Abate, A.; Zakeeruddin, S. M.; Luo, J.; Mayer, M. T.; Gr?tzel, M. *Nat. Commun.* **2015**, *6*, 7326.

(13) Kumar, B.; Atla, V.; Brian, J. P.; Kumari, S.; Nguyen, T. Q.; Sunkara, M.; Spurgeon, J. M. *Angew. Chemie Int. Ed.* **2017**, *56* (13), 3645–3649.

(14) Zhu, W.; Zhang, Y.-J.; Zhang, H.; Lv, H.; Li, Q.; Michalsky, R.; Peterson, A. a; Sun, S. *J. Am. Chem. Soc.* **2014**, *136* (46), 16132–16135.

(15) Liu, M.; Pang, Y.; Zhang, B.; De Luna, P.; Voznyy, O.; Xu, J.; Zheng, X.; Dinh, C. T.; Fan, F.; Cao, C.; de Arquer, F. P. G.; Safaei, T. S.; Mepham, A.; Klinkova, A.; Kumacheva, E.; Filleter, T.; Sinton, D.; Kelley, S. O.; Sargent, E. H. *Nature* **2016**, *537* (7620), 382–386.

(16) Wu, J.; Yadav, R. M.; Liu, M.; Sharma, P. P.; Tiwary, C. S.; Ma, L.; Zou, X.; Zhou, X.-D.; Yakobson, B. I.; Lou, J.; Ajayan, P. M. *ACS Nano* **2015**, *9* (5), 5364–5371.

(17) Rasul, S.; Anjum, D. H.; Jedidi, A.; Minenkov, Y.; Cavallo, L.; Takanabe, K. *Angew. Chemie Int. Ed.* **2015**, *54* (7), 2146–2150.

(18) Sarfraz, S.; Garcia-Esparza, A. T.; Jedidi, A.; Cavallo, L.; Takanabe, K. *ACS Catal.* **2016**, *6* (5), 2842–2851.

(19) Zhao, Y.; Wang, C.; Wallace, G. G. *J. Mater. Chem. A* **2016**, *4* (27), 10710–10718.

(20) Li, M.; Wang, J.; Li, P.; Chang, K.; Li, C.; Wang, T.; Jiang, B.; Zhang, H.; Liu, H.; Yamauchi, Y.; Umezawa, N.; Ye, J. *J. Mater. Chem. A* **2016**, *4* (13), 4776–4782.

(21) Yin, Z.; Gao, D.; Yao, S.; Zhao, B.; Cai, F.; Lin, L.; Tang, P.; Zhai, P.; Wang, G.; Ma, D.; Bao, X. *Nano Energy* **2016**, *27*, 35–43.

(22) Zhang, X.; Wu, Z.; Zhang, X.; Li, L.; Li, Y.; Xu, H.; Li, X.; Yu, X.; Zhang, Z.; Liang, Y.; Wang, H. *Nat. Commun.* **2017**, *8* (March), 14675.

(23) Larrazábal, G. O.; Martín, A. J.; Mitchell, S.; Hauert, R.; Pérez-Ramírez, J. *J. Catal.* **2016**, *343*, 266–277.

(24) Rosen, J.; Hutchings, G. S.; Lu, Q.; Rivera, S.; Zhou, Y.; Vlachos, D. G.; Jiao, F. *ACS Catal.* **2015**, *5* (7), 4293–4299.

(25) Blizanac, B. B.; Ross, P. N.; Marković, N. M. *J. Phys. Chem. B* **2006**, *110* (10), 4735–4741.

(26) Jovic, B. .; Jovic, V. .; Stafford, G. . *Electrochem. commun.* **1999**, *1* (6), 247–251.

(27) Horswell, S. L.; Pinheiro, A. L. N.; Savinova, E. R.; Danckwerts, M.; Pettinger, B.; Zei, M.-S.; Ertl, G. *Langmuir* **2004**, *20* (25), 10970–10981.